Journal of Bio-optics
https://www.sciltp.com/journals/jbo

Review

Eccentric Infrared Photorefraction: A Review of Evolution, Optical Design, Features and Applications

Shrikant R. Bharadwaj [1,2,*], Silvestre Manzanera [3] and Pablo Artal [3]

[1] Brien Holden Institute of Optometry and Vision Sciences, L V Prasad Eye Institute, Hyderabad 500034, India
[2] Prof. Brien Holden Eye Research Centre, L V Prasad Eye Institute, Hyderabad 500034, India
[3] Laboratorio de Optica, Universidad de Murcia, 30100 Murcia, Spain
* Correspondence: bharadwaj@lvpei.org

How To Cite: Bharadwaj, S.R.; Manzanera, S.; Artal, P. Eccentric Infrared Photorefraction: A Review of Evolution, Optical Design, Features and Applications. *Journal of Bio-optics* **2025**, *1*(1), 4.

Received: 15 May 2025
Revised: 19 June 2025
Accepted: 1 July 2025
Published: 9 July 2025

Abstract: Photorefraction is seven-decade old technology that allows objective and non-invasive estimation of the eye's refractive error using retro-illuminated photographs of the pupil. A special variant of this technique—*eccentric infrared photorefraction*—has now become the technology of choice for the screening of uncorrected refractive errors and other amblyogenic factors in the pediatric population. Eccentric infrared photorefraction is also the preferred measurement tool for scientific investigations on the physiology and pathobiology of the near-triadic reflex (accommodation, convergence and pupil miosis). Broadly, this technique uses an extended near-infrared light source that is mounted eccentric to the camera aperture to illuminate the retina. The optically double-pass reflected light generates a retro-illuminated luminance profile across the pupil, the gradient of which may be used to estimate the eye's refractive power using standard calibration techniques. The present review summarizes the origins of photorefraction and then delves into the optical principles of eccentric infrared photorefraction, its properties, calibration techniques and associated pitfalls. The review also discusses the present and future use-cases of this technology. Overall, this review provides the basics of photorefraction for early readers of this topic and offers some practical guidelines for the moderate to advanced users of this technique.

Keywords: amblyopia; defocus; pediatric eye screening; keratoconus; retro-illumination; uncorrected refractive errors

1. Introduction

Photorefraction refers to a family of techniques that are used to estimate refractive errors using retro-illuminated photographs of the eye [1]. The origins of this technique may be traced back to an internal report for the MIT Research Laboratory of Electronics by Howland & Howland in 1962 [1]. Their apparatus consisted of four cylindrical lens segments placed in front of a camera and arranged in such a way that the illuminated image of the fundus reflex appeared as a cross in the pupil plane. The dimensions of this cross was an indicator of the eye's refractive error. With the advent of fiber optics, the original apparatus was miniaturized in size and complexity, leading to the development of a technique called *orthogonal photorefraction* [2]. This was closely followed by a variant—*isotropic photorefraction*—in which the eye's refractive error was obtained by comparing the size and shape of the fundus reflex that appear in the pupil in two images, one focused before and another after the pupil's plane [2]. These two are modalities of *on-axis photorefraction* because the camera and the light source are coaxial with the optical axis of the eye.

Independently, Kaakinen [3,4] invented and subsequently Bobier [5], Norcia [6], Schaeffel [7] and colleagues described the technique of *eccentric photorefraction*, wherein the light source was positioned outside the optical axis of the eye. This technique greatly simplified the optical setup because now the light source can be the *flash device used in photography to capture photographs under dim conditions*, positioned at a desired distance away from the camera center. This technique also resembles the oft-used retro-illumination method of examining the eye in a slit-lamp biomicroscope wherein the light source is purposefully moved eccentrically, relative to the optical axis of the instrument [8]. The visible light source in this technique was eventually replaced with near-infrared light sources that avoided pupillary miosis and offered increased comfort for the participant undergoing the measurements [7,9]. The refractive state of the eye is codified differently in eccentric photorefraction compared to its on-axis equivalent. The fundus reflex formed across the pupil in eccentric photorefraction resembles the shape of a crescent moon in its waxing gibbous phase. The shape of this photorefraction crescent may be calibrated such that the eye's refractive error or its changes with viewing condition could be directly read off in diopters [7,9]. Since then, several theoretical and practical aspects of the eccentric photorefraction technique including its dead-zone and saturation limits, impact of the eye's wavefront aberrations and factors that influence the calibration profile have been discussed in detail in the literature [10–13]. The purpose of this review is to summarize the literature on the basic optical principles of photorefraction, its calibration properties and the present utility and prospects.

Today, eccentric infrared photorefraction has become the technique of choice for the screening of refractive errors and other amblyogenic factors (e.g., strabismus) in the pediatric population [14–16]. Photorefraction has also become the technique of choice for vision scientists studying the accommodative and near-triadic (accommodation, binocular convergence and pupil miosis) behavior in typically and atypically developing children [7,17–20], and for animal biologists interested in accommodation and refractive error development [21–27]. At least four different variants of the photorefraction device are now commercially available for human use (e.g., A12C and A12R, Plusoptix GmbH, Nuremberg, Germany; Spot Vision Screener, Welch Allyn, Chicago, USA; GoCheck Kids, Nashville, USA; iScreen Vision, Cordova, USA) and for use in small animals such as mice and chickens (e.g., photorefractor from StriaTech, Tübingen, Germany). The aforesaid status enjoyed by photorefraction arises from the following advantages this technique has to offer over retinoscopy and other autorefraction techniques:

(1) The eye's refractive power may be estimated in photorefraction from a *remote working distance* (typically, 1m in humans), a feature that is valuable when evaluating uncooperative children. Measurements in other autorefractor designs are also obtained non-invasively like photorefraction, albeit, from a much closer distance to the eye.
(2) The photorefractor is typically *hand-held and portable*, enabling its use in mass eye screening endeavors. Other autorefractor designs are typically table-top mounted and not easily portable.
(3) The refractive error output of photorefraction is typically *immune to small misalignments between the camera and the eye*. This too is an advantage when dealing with children and animals, both of whom cannot be instructed to fixate onto a specific target.
(4) That the photorefractor (and other autorefractor designs too) operates using *near-infrared light source* (typically, using LEDs with 850 nm of peak spectral emittance), allows measurements to be made with maximal biological pupil dilation. This is significantly advantageous over retinoscopy that uses visible light, producing significant pupillary miosis and discomfort to the observer.
(5) Unlike other autorefractor designs, *simultaneous bilateral refraction* is possible in photorefraction, enhancing efficiency of refraction measurements during eye examinations.
(6) In addition to the eye's refractive power, *synchronous estimation of gaze position and pupil size* is possible in photorefraction. This is of tremendous value whilst studying the near triad synchronously, in all its complexity.
(7) The retro-illumination reflex that forms the basis for the photorefraction technique may also *identify other ophthalmic pathologies* such as media opacities (e.g., cataract [28]) or optical defects arising from corneal/lenticular distortions (e.g., keratoconus [29,30]).

2. Basic Principles

2.1. Description of the Photorefraction Crescent for a Point-Like Light Source

In eccentric photorefraction, the fundus reflex imaged at the eye's pupil plane occupies only a part of the pupil, resulting in a luminance crescent across the pupil (Figure 1A). In the first pass, when a point source of light enters the eye, it forms an image on the retina, the distribution of which is dependent on diffraction effect from the pupil edges and wavefront aberrations from the aspherical refractive surfaces [31]. Consequently, a variable-sized spot of light is observed on the retina. In the second pass, assuming that the retina is a Lambertian reflector [32], each illuminated point emits light in all directions toward the pupil. Of these, the light rays passing through the pupil and the camera aperture contribute to the crescent formation. The crescent properties can be estimated by determining, for each location in the pupil, which rays both intersect the pupil at that location and cross the camera aperture. To this end, Howland's analysis [33] can be applied and rely on the fact that if a ray crosses the aperture at some point, the same ray will cross the image of the aperture formed by the eye's optics at the conjugate point. Figure 1B offers a schema of this configuration for a myopic eye, in which the image of the camera aperture is on a plane anterior to the retina. The rays intersecting the pupil at any given point are those encapsulated within a cone, with its vertex at that point and a width determined by the size of the aperture's image. The intersection of this cone with the retina dictates the extent of the emitting locations on the retina, contributing to the brightness of the corresponding point in the pupil. Figure 1B shows three such points that are useful to assess the vertical intensity profile of the crescent across the pupil. Point A does not collect any light as there are no emitting points on the retina within the corresponding cone. However, point A in Figure 1B establishes the beginning of the crescent for the base of the cone and the spot on the retina are tangential, signifying that any point below point A will begin to exhibit some luminosity. The base of the cone corresponding to point B in Figure 1B partially overlaps the retinal spot, with the extent of this overlap increasing as we descend within the pupil. The spatial region characterized by partial overlap results in a progressively rising intensity profile for the crescent. At a certain point on the pupil, the base of its corresponding cone and the retinal spot fully overlap (see point C in Figure 1B), resulting in the attainment of the highest intensity within the crescent.

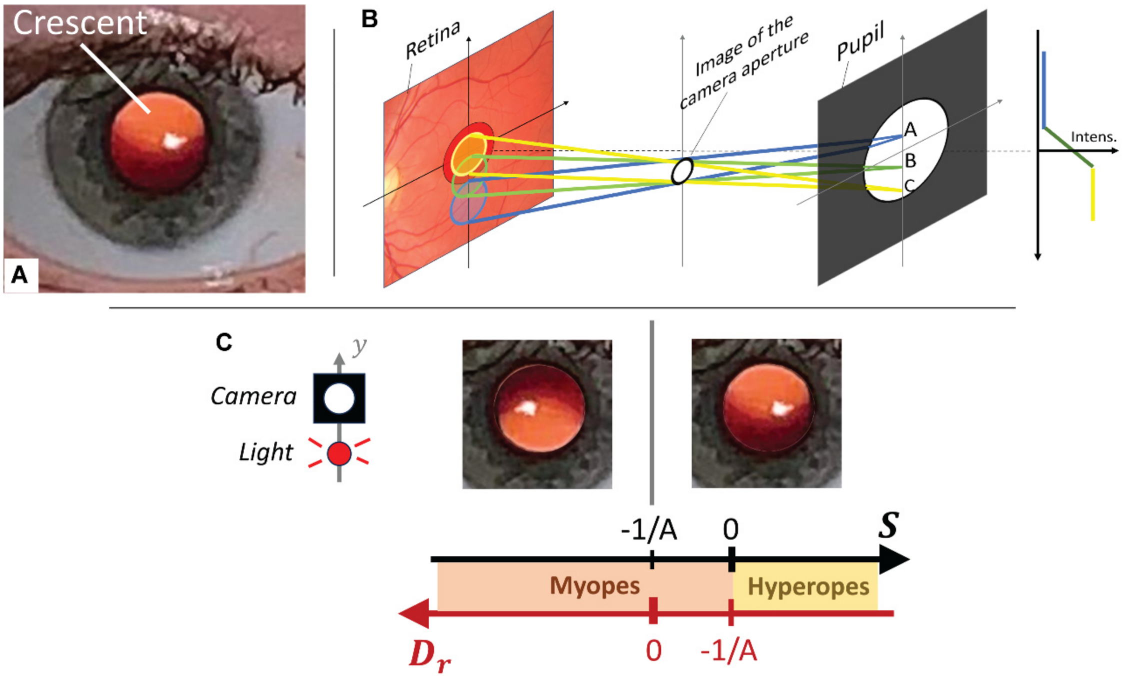

Figure 1. Panel (**A**) Example of the characteristic fundus crescent found in eccentric photorefraction with the use of a single point-like light source. Panel (**B**) Illustration of the photorefraction crescent formation in a myopic eye. The light source (not shown) is on the optical axis and produces a spot (red circle) of light on the retina in the first pass. Reflection of light from the retinal spot radiates in all directions but only those passing through both the pupil and the camera aperture (or its image formed by the eye) contribute to the brightness in the pupil. These points lie within the intersection between the retinal spot and the cone formed by the point in the pupil and the image of the aperture. Points A, B, and C serve as an example of the different scenarios that can occur in the crescent profile (shown on the right side): null (A), increasing (B), and constant intensity (C). Panel (**C**) Relationship between relative defocus and the spherical error in photorefraction. Two images illustrating examples of crescents produced by opposite relative defocus are displayed in the upper part of the figure. If the light source were above the camera aperture, the two images would be exchanged.

The appearance of the crescent depends on the refractive state of the eye relative to the working distance (A) between the light source and the eye (Figure 1C), because both parameters determine the size of the retinal spot. Therefore, the crescent formation is better described in terms of the defocus of the eye (reciprocal of the distance to the far point) relative to the defocus induced by the proximity of the light source ($1/A$) [34]. This relative defocus (D_r) can be mathematically expressed in terms of the spherical refractive error S of the eye ($S < 0$ for myopes; $S > 0$ for hyperopes) as follows:

$$D_r = -\left(S + \frac{1}{A}\right) \quad (1)$$

Note that in Equation (1), for a myopic eye with $S = -1/A$, $D_r = 0$. Note also that D_r refers to a defocus, while S refers to a correction, as indicated by the negative sign in the equation. Figure 1C illustrates the relationship between the relative defocus and the spherical error. All hyperopic eyes have $D_r < -1/A$, while all myopic eyes have $D_r > -1/A$. The value $D_r = 0$ represents a turning point for the orientation of the crescent within the pupil. The upper part of Figure 1C shows examples of crescents for positive and negative relative defocus, illustrating the different orientations.

2.1. Description of the Luminance Slope Formation for an Extended Light Source

The crescent formation for an extended light source can be conceptually understood using a similar approach to that used for point-like sources (Figure 2). An extended light source can be thought of as a combination of multiple point-like sources. In the first pass, each of the point-like sources creates overlapping retinal spots. Their combined effect produces an intensity distribution with a central area of constant intensity that fades smoothly to zero at the edges, as illustrated in Figure 2A. Recall that, for a point-like source, the retinal spot declines abruptly to zero at the edge. Now, in the second pass (Figure 2B), the larger retinal spot causes the beginning of the crescent to shift, resulting in a wider crescent. Simultaneously, the gradually declining intensity within the retinal spot increases the area of points in the pupil that collect increasing amounts of light from the retina. The resulting intensity distribution in the pupil takes the form of an extended intensity gradient. Schaeffel et al. [7] used rows of LEDs arranged at different eccentricities that simultaneously illuminated the eye to perform real-time measurement of accommodation in humans. This arrangement is equivalent to an extended light source and has been adopted in all the commercial designs of photorefractors noted in Section 1. Schaeffel et al. [7] found an almost linear intensity gradient in the crescent, with its slope showing a clear dependency with the eye's refractive state.

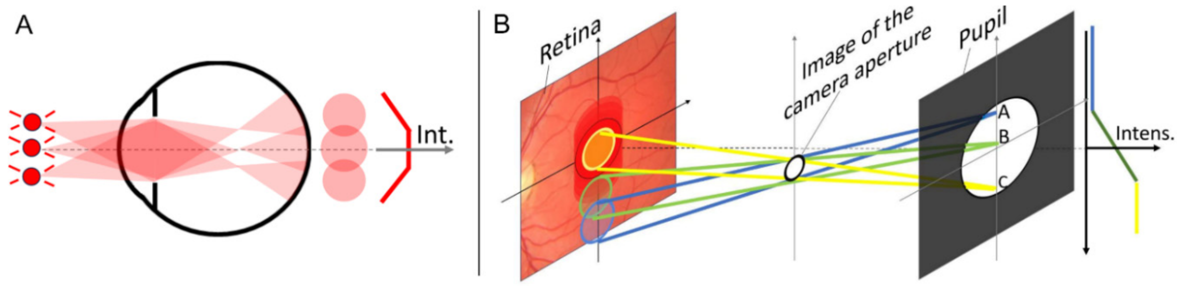

Figure 2. Photorefraction crescent formation in a myopic eye for an extended light source, which can be modeled as multiple point-like sources. Panel (**A**) In the first pass, each individual light source creates a retinal spot. The combined effect of all these sources is a larger retinal spot with an intensity distribution that gradually increases towards the center. Panel (**B**) In the second pass, the enlarged retinal spot shifts the beginning of the crescent (point A) resulting in a wider crescent. Additionally, the gradually declining intensity distribution within the spot increases the area of the pupil that collects light with varying intensity, as exemplified by point B.

3. Obtaining Refraction Estimates from the Luminance Gradient of the Crescent

Early studies using eccentric photorefraction used a point-like light source and relied on the extent of the crescent as the parameter to retrieve the refractive state of the eye [3,5,6,33]. This was a preferred parameter because measuring the extent of the crescent is simple, and there are available equations relating this parameter with the spherical error of the eye. However, such a calculation is limited in that the precise detection of the crescent edge can be erroneous owing to the pupil appearing illuminated overall from the light scattered in the eye. Additionally, the presence of higher-order aberrations in the eye also affects the photorefraction intensity distribution, obscuring a precise calculation of the crescent location [11–13]. Finally, the relationship between the extent of the crescent and the corresponding spherical refractive error is not linear—the crescent grows quickly for small values of the refractive error and asymptotes for larger values. These issues prevented the technique based on a single point-like light source from being automated [7].

Based on the work by Schaeffel et al. [7], this challenge is overcome in present-day photorefractors by using an extended light source and considering the readily estimable luminance gradient formed across the pupil (Figure 3A–E). This luminance gradient remains largely linear in eyes with regular refractive error and, its slope, obtained using standard least-square linear regression analysis over the central 80% of the pupil area, tends to be directly proportional to the magnitude of refractive error (Figures 3F–O) [7,10,30,35]. As illustrated earlier, the polarity of this luminance gradient is dependent on the relative locations of the camera and the light source—for a schema where the camera is placed above the light source, the luminance gradient for hyperopia eyes progressively increases from the bottom to the top of the pupil (Figure 3A,F,K) while the luminance gradient for myopia eyes shows the opposite trend (Figure 3C–E,H–J,M–O). Emmetropic eyes do not show any such gradient, and the eye is uniformly illuminated from the scattered light reflected from the retina (Figure 3B,G,L). Identical analyses can be applied to an eye accommodating to a near target, wherein the increased myopic luminance profile may indicate the magnitude of the accommodative response [7,19,36]. The linearity of these profiles across the pupil in eyes with refractive errors are evident in the 3D and 2D plots shown in Figure 3F–J,K–O, respectively.

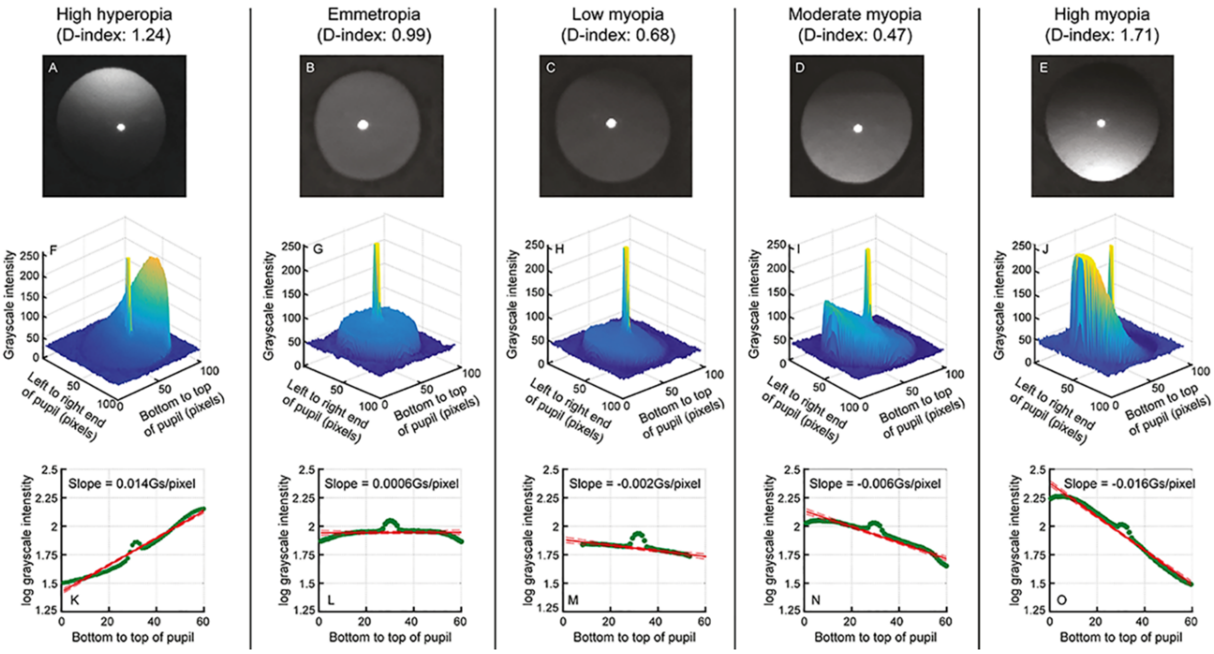

Figure 3. Eccentric infrared photorefraction profiles obtained in representative eyes with high hyperopia, emmetropia, and low to high myopia. Panels (**A**–**E**) represent the actual photorefraction profile from these eyes. Panels (**F**–**J**) show 3D surf plots of the luminance profile distribution across the pupils. Panels (**K**–**O**) show the same luminance gradient plots, this time collapsed across the horizontal extent of the pupil, making it amenable to 2D linear regression fitting. The bright spot in each photorefraction profile is the 1st Purkinje image and this is routinely used to determine the gaze position of the eye, using standard Hirschberg ratio calculations [37,38]. In all these images, the camera was placed above a 4 × 6 rectangular array of infrared LED light sources. Images were captured from a viewing distance of 1 m. Figure adopted from Patel et al. (2022) [30].

3.1. Absolute and Relative Calibration of the Slope-Based Photorefraction Profile

The photorefraction technique is used (1) to accurately estimate the absolute value of the eye's sphero-cylindrical refractive error and (2) to accurately estimate the change in refraction values from one viewing state to another. The former has value in eye screening endeavors or cohort-level studies that measure the absolute value of a refractive error [14,16,39,40] or accommodative lag [41–43] while the latter is useful in cross-sectional studies that measure the gain of accommodation [7,19,36,44] or in studies that measure longitudinal changes in the eye's refractive error state [21,23–27]. That these purposes are met is critically dependent on the calibration of the photorefraction luminance profile into units of diopters. Two different techniques have been described in the literature towards this end—an *absolute calibration technique* meant for the former purpose and a *relative calibration technique* meant for the latter purpose. The readers are referred to papers by Blade and Candy [45], Schaeffel et al. [7] and Bharadwaj et al. [10] for a detailed description of these techniques. Briefly, the absolute calibration technique involves comparing the refractive output of the photorefractor to a standard technique like retinoscopy [45]. Relative calibration involves precise estimation of the rate of change of the luminance gradient per unit change in the eye's dioptric power [7,10,45]. Absolute calibration is technically more challenging and cumbersome to conduct, compared to relative calibration. Therefore, the relative calibration technique and its dependencies have been explored in greater detail in the literature (See Section 3.2 for details). Most studies in literature that use commercial photorefractors perform the relative calibration procedure to gain certainty about the change in refractive power estimates in their measurements. These studies either assume that their device is either accurate for absolute measures of refractive error or they refrain from making any claims about the absolute refractive error state of the eye.

Relative calibration of photorefraction may be readily achieved using straightforward empirical protocols. While different variants of this protocol are available in the literature [10,20,45–47], all of these, in principle, involve inducing known values of myopia and hyperopic refractive errors before the eye and obtaining a luminance gradient for each of these errors (Figure 4A). The luminance gradient (in units of grayscale luminance/pixel) difference between the two eyes is then calculated for each lens power and the resultant anisometropia is regressed against the induced refractive error values (in diopters) to obtain the calibration function (Figure 4B). The slope of this function is the calibration factor, which is used to scale the raw data for accurate estimates of refractive power changes.

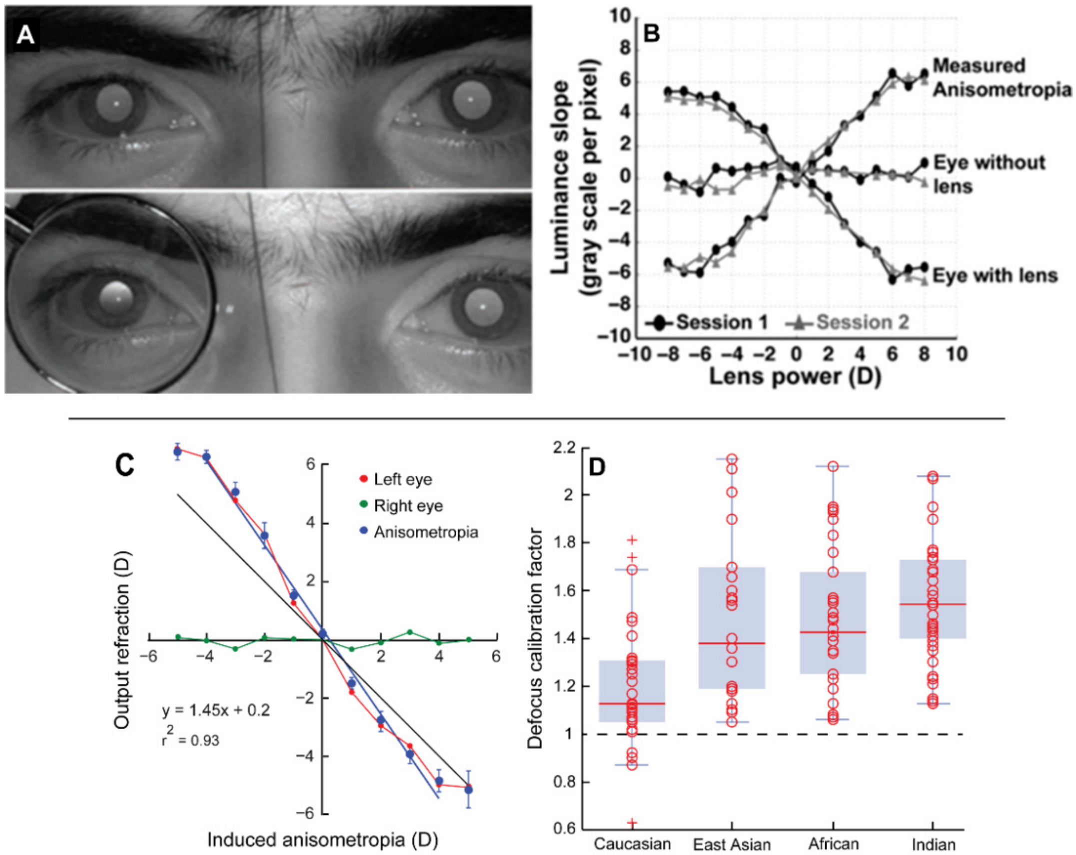

Figure 4. Panel (**A**) Representative images of a participant on whom the relative calibration of the photorefraction luminance gradient is performed. The top image shows the right eye occluded using an infrared transmitting filter while the fellow eye is open and fixated on a target. The bottom image shows the same set up but with a negative lens before the occluded eye. The photorefraction luminance gradient corresponding to the induced hyperopia is apparent in the bottom image, even while the profile of the fellow eye remains unchanged. Panel (**B**) A representative photorefraction calibration function obtained by placing trial lenses before the infrared filter occluded eye. The resultant anisometropia in the luminance profile slopes was regressed against the trial lens power over the linear portion of the data (note the saturation of luminance profiles beyond ±7D) to obtain the calibration factor. Data from two calibration sessions on the same participant are shown here to demonstrate measurement repeatability. Panel (**B**) is adapted with permission from Bharadwaj et al. [10] © Optica Publishing Group. Panel (**C**) A representative photorefraction calibration profile obtained from a commercial photorefractor that reads-out the data in units of diopters. The protocol for deriving this calibration profile is identical to panel (**B**), but with both the abscissa and ordinate variables represented in diopters. Panel (**D**) Box and Whisker plot showing the distribution of defocus calibration factors in different ethnic groups tested by Sravani et al. [35]. The solid red line shows the median defocus calibration factor of that ethnic group, and the box boundaries and error bars show the data variance. The dashed black line indicates a unity defocus calibration factor (i.e., when the output anisometropia equals the input lens power in panel (**A**) of this figure). Panels (**C**,**D**) are adapted with permission from Sravani et al. [35] © Nature Publishing Group.

Estimations of astigmatism are also performed by utilizing the slope in the intensity profile. This slope only provides information about the refractive error along the meridian defined by the line connecting the light source and the center of the camera aperture. This method is sufficient to obtain a measurement for an eye with only a rotationally symmetrical refractive error such as defocus. However, for an eye with astigmatism, it's necessary to use rows of LEDs oriented at multiple meridians, as described by Gekeler et al. (1997) [48]. The values obtained from these measurements are then combined to produce a full refraction, comprising sphere, cylinder, and axis.

3.2. Determinants of the Relative Calibration Function of Eccentric Infrared Photorefraction

In practice, the relative calibration factor may be influenced by several parameters, some of which are easily controllable while others are not. In general, this photorefraction calibration factor does not vary significantly with age, uncorrected refractive error or viewing distance [13,46]. The ensuing section describes the parameters that may influence the calibration factor.

3.2.1. Ocular Accommodation

Placing a trial lens before the eye for epochs that exceed the latency period of the accommodative step response (~300–500 ms in human adults and infants [49,50]), invariably runs the risk of stimulating the eye's accommodation during the calibration process. This is undesirable, for the photorefraction gradients may no longer represent the impact of only the induced trial lens but some combination of the induced lens power plus the resultant change in accommodation. This is avoided in the calibration protocol by typically occluding the eye that is to be calibrated using an infrared transmitting filter that eliminates form vision (thus negating blur-driven accommodation) even while the photorefractor continues recording the refraction values through the lens (Figure 4A). The fellow eye remains open and this helps with stable fixation at a distant object. However, the infrared light emitting diodes of the photorefractor remain visible through the infrared transmitting filter and an assumption is made that this target does not trigger blur-feedback to impact the resultant calibration function. As a second check on accommodation, the photorefraction luminance gradients of both eyes—the infrared filter occluded eye with the trial lens and the fixating eye—are recorded simultaneously and the resultant interocular difference in the luminance gradients ("measured anisometropia" in Figure 4B) is plotted against the induced trial lens for obtaining the calibration function. This protocol assumes that the accommodative responses in the two eyes are consensual [51] and the net anisometropia obtained for a given trial lens will remain unimpacted even if the accommodation varies through the calibration protocol. As such, the calibration measures obtained using this technique are quite repeatable (Figure 4B), but the readers are referred to Bharadwaj et al. [10] for a detailed treatment on the inter- and intra-subject variability of the calibration function. While this protocol may offer immunity to the calibration estimates against accommodative changes, the protocol may not be straightforward to implement in children who are resistant to occlusion or in those with strabismus, wherein the eye might deviate under occlusion [47], or in those with only one functional eye [52] or in the rare instances where the accommodative responses are indeed bilaterally dissimilar (notwithstanding confounding factors such as artefacts from peripheral refraction, eye movements and oblique astigmatism arising from the experimental set up) [20]. Under such circumstances, the trial lenses may be introduced before the eye for much shorter epochs and the change in the eye's refractive power before initiation of the accommodative response may be considered for calibration.

Commercial photorefractors often have the calibration factor built into their algorithm, enabling the devices to directly report the refractive error estimates in diopters. The calibration factor may be derived during device development by employing a protocol such as the one described above and incorporating the population-average value into the algorithm. As will be seen in the section below, there are reasons to believe that this population-average calibration factor may not be accurate at all times—an individual calibration is thus recommended to verify the output of the refractive error estimates obtained from the photorefractor. Under such circumstances, the same calibration protocol described above may be repeated, except that the calibration function will plot the observed anisometropia against the induced anisometropia, with both anisometropia values represented in dioptric units (Figure 4C). The slope of this function—a unitless entity—can be used as a scaling factor to adjust the raw data obtained from the photorefraction device [35].

3.2.2. Ethnicity

Bharadwaj and colleagues reported ethnicity-dependent variability in the calibration factor [10,35]. The calibration factors were higher for those with Indian and African descent, relative to those with European Caucasian descent (Figure 4D). The calibration factors of East Asian eyes were somewhere in between that of the other two cohorts (Figure 4D). While the exact reason for this difference remains unknown, obvious factors like eye color and pupil size were ruled out as contributors to this variability in their study [35]. This ethnicity-dependent difference in the calibration factor does induce a significant magnitude of error in the refractive error estimates obtained using photorefraction. For instance, in the Sravani et al. study, the errors were as high as 51% over-estimation of the refractive error in Indian eyes when the built-in calibration factor was used for estimation (presumably obtained from Caucasian eyes, based on the device's origin in Nuremberg, Germany) [35]. A more recent study by Pophal et al. [53] found the sensitivity/specificity of a commercial photorefractor in detecting uncorrected refractive errors in a pediatric population to vary based on skin pigmentation. Based on these results, the authors of this study asserted the need for considering ethnic and racial diversity in future advances of the photorefractor technology. This suggestion could simply be incorporated by having ethnicity-dependent calibration factors built into the software of these commercial photorefractors and choosing the appropriate calibration factor from a drop-down list of the device's software interface prior to data collection. A second undesired consequence of this ethnic variability is the saturation of the photorefraction profiles at earlier dioptric values in eyes with higher calibration factors, compared to those with lower calibration factors. Unfortunately, this issue effectively narrows the operating range of the photorefractor in the former cohorts, relative to the latter [10,35].

3.2.3. Pupil Size and Fundus Reflectance

A third factor that influences the photorefraction calibration values is the overall brightness of luminance profile, as determined by the eye's fundus reflectivity and pupil size. Eyes with lower fundus reflectivity and smaller pupil sizes result in duller photorefraction profiles, relative to those at the other end of the spectrum. The luminance slope for the former category may be shallower than those of latter, leading to erroneous estimates of refractive error (Figure 5, for pupil size dependency) [13]. This is typically corrected by performing a grayscale luminance gain correction on the photorefraction images, prior to the slope calculation. Fortunately, commercial photorefractors have this gain correction built-into their software and the average user of these devices need not be concerned much about this issue. Investigators who embark on building their own photorefractor should, however, consider this as a critical step in their software development process. Expectedly, there is a limit to which the gain correction process can fix the overall brightness of the photorefraction reflex. Images obtained over very small (<2.5–3 mm) or very large (>7.5 mm) pupil diameters may not be fixable with this process—the reflex may be too dark in the former category for meaningful estimation of the luminance slope while the reflex may be saturated in the latter category to perform the same operation [13]. Commercial photorefractors therefore tend to impose a pupil size range limitation on their device functionality—pupil diameters between 3 and 7 mm, typically, fall within the operating range of most commercial photorefractors. As a practical tip, saturation of the photorefraction profile owing to large pupil diameters may be overcome by turning the room lights on to produce pupillary miosis or reducing the camera aperture (for custom-designed photorefractors) or reducing the camera's gain in the device software (for commercial and custom-designed photorefractors).

A brighter than usual photorefraction reflex may be observed when the infrared camera capturing this reflex becomes on-axis with the eye's optic nerve, more so when the pupils are dilated than undilated. This is evident in Figure 6, wherein the photorefraction reflexes are uniformly bright in both eyes during primary gaze when the camera is largely on-axis to the two eyes (Figure 5A). Yet, when the eyes move to ~15° of *levoversion* or dextroversion position, the optic nerve of the right and left eye become on-axis with the camera, respectively, leading to bright photorefraction reflexes in these eyes (Figure 5B,C). When gain is corrected, the bright photorefraction reflex shows a myopic luminance distribution across the pupil, as seen in Figure 5D. This issue may need to be factored in while using the eccentric infrared photorefraction technique for estimating the peripheral refraction of the eye (Figure 5D) [54,55]. Interestingly, similar observations are reported in off-axis visible light photography, wherein reflections from the optic nerve manifest as unilateral leukocoria in otherwise healthy eyes, often confusing with ophthalmic pathologies like retinoblastoma [56,57].

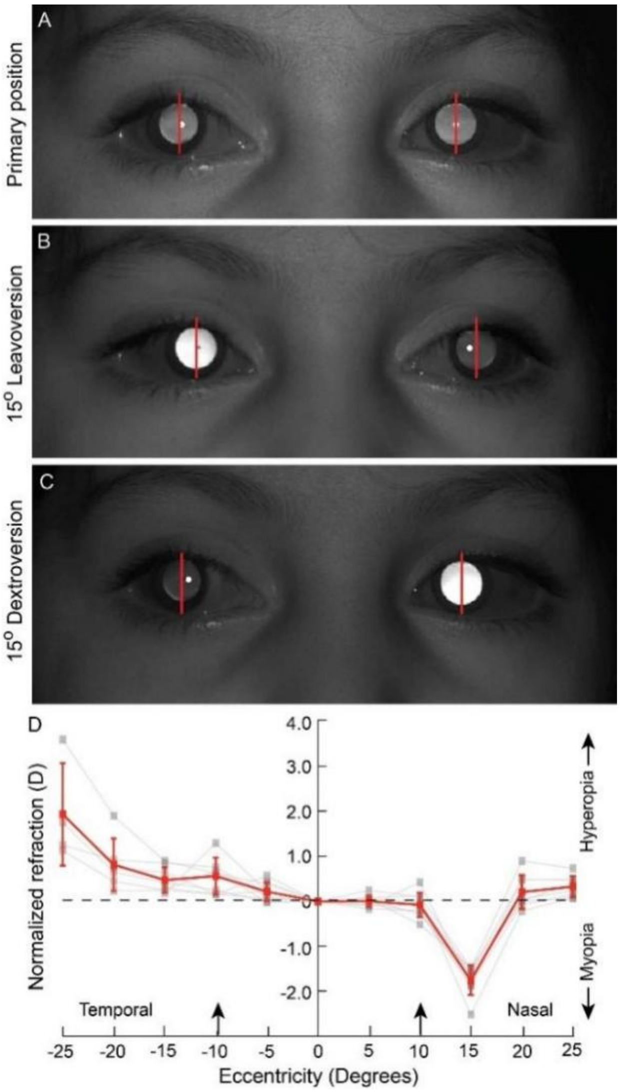

Figure 5. Bilateral eccentric infrared photorefraction profiles obtained from primary position of gaze (panel **A**) and from ~15° of levoversion (panel **B**) and dextroversion (panel **C**). The photorefraction reflex increases in brightness in the eye whose optic nerve becomes on-axis with the camera. Panel **D**) Mean (±1SD) (red trace) and individual (gray traces) normalized photorefraction values obtained across the vertical meridian of the pupil plotted as a function of gaze eccentricity for five individuals. The photorefraction reflex shifts towards a myopic value at ~15° of nasal gaze position, wherein the optic nerve becomes on-axis with the photorefractor.

3.2.4. Higher-Order Wavefront Aberrations

The impact of higher-order wavefront aberrations on the photorefraction luminance profile has been reported in detail by Roorda and colleagues [11,12] and, more recently, by Wu et al. [13]. In general, their influence ranges from simply shifting the entire calibration along the dioptric axis (for radially symmetric Zernike polynomials like spherical aberration) to altering the linearity of the luminance profile formed across the pupil (for radially asymmetric Zernike polynomials like coma or trefoil) (see Figure 6 in Wu et al. [13]). These effects are expected to scale with the pupil size, owing to an overall increase in the magnitude of the wavefront aberrations. In an otherwise optically healthy eye, the magnitude of these higher-order wavefront terms is small [31] and thus the influence of higher-order wavefront aberrations on the photorefraction profile is likely to be negligible. Their impact, on the other hand, is likely to be more pronounced in eyes with distorted optics (e.g., keratoconus [58,59], keratorefractive surgeries [60,61]). Such non-linearities in the photorefraction luminance profile have been identified in eyes with keratoconus [29,30] and they have been quantified as a means of detecting this disease condition using photorefraction, vis-à-vis, standard corneal tomography (Figure 6) [30]. These profiles have also been recently used to train artificial intelligence and deep learning models for further enhancing the diagnostic capability of photorefraction in detecting keratoconus [62]. However, with such significant non-linearities, the photorefraction profile may not even be meaningfully calibrated using the protocols described earlier (Figure 4).

Thus, this technology's primary use as an objective estimator of the eye's sphero-cylindrical refractive error may remain unfulfilled in such highly distorted eyes.

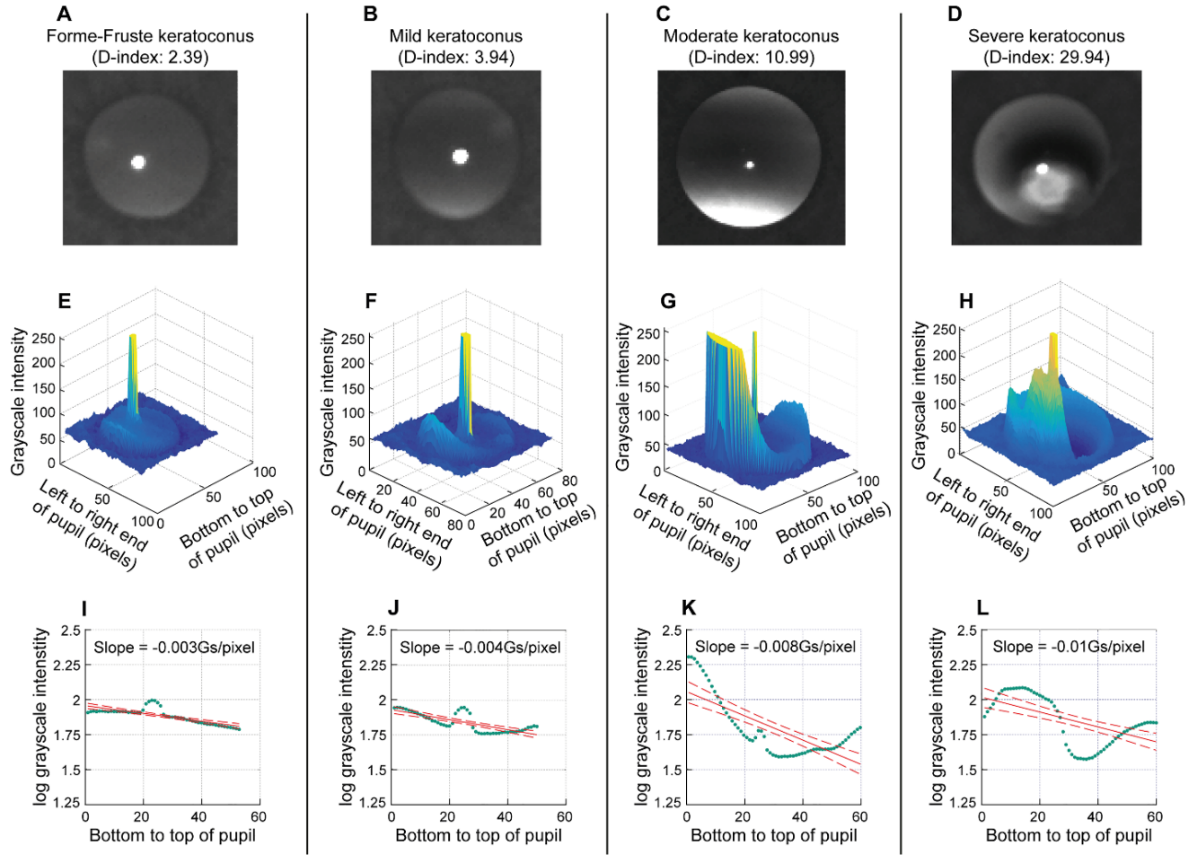

Figure 6. Sample eccentric infrared photorefraction profiles obtained in eyes with different grades of keratoconus. Panels (**A**–**L**) are identical in representation to Figure 3. The non-linearity in the luminance profile across the pupils is evident in these panels, especially for the mild to severe keratoconics. Figure adopted from Patel et al. (2022) [30].

3.2.5. Optical Magnification

In addition to inducing defocus, the trial lenses used for calibrating the photorefractor also induce magnification/minification of the entrance pupil of the eye over which the luminance gradient is computed (Figure 7A) [63]. Bharadwaj et al. [64] and Wu et al. [13] showed that this image magnification influences the photorefraction luminance profile by artefactually shallowing the profile for positive lenses and steepening the profile for negative lenses (Figure 7B). The myopic defoci induced by the positive lenses will be underestimated because of image magnification while the hyperopic defoci induced by the negative lenses will be overestimated because of image minification (Figure 7C). Indeed, Bharadwaj et al. [64] showed that the refractive error output for myopic eyes by a commercially-available photorefractor could be systematically manipulated by placing afocal magnifiers lenses before the eye—the myopia is underestimated with image magnification and overestimated with image minification, all relative to the eye without magnifiers (Figure 7D,E) [64]. Given that these magnification effects gain prominence with increased lens powers and with increasing vertex distances, caution is to be exercised while using high powered lenses at large vertex distances for calibration purposes [10,35]. Similar caution may also need to be exercised while performing photorefraction through the spectacle correction of individuals (e.g., when estimating the accommodative capability with best-corrected spectacles in children with Down syndrome [65,66]). The data may need to be corrected for the magnification effect, using the formula described in Bharadwaj et al. (2018) [64].

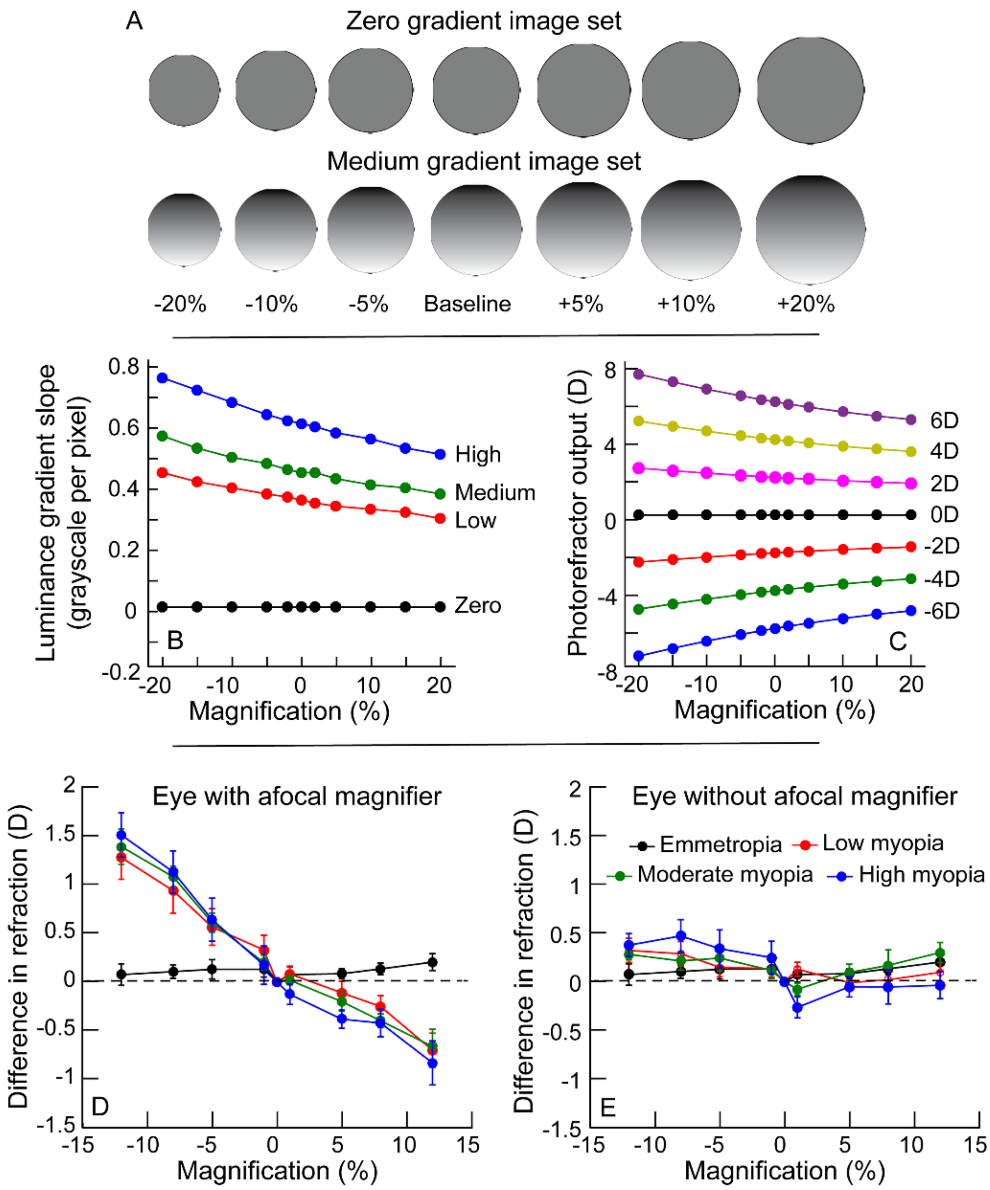

Figure 7. Panel (**A**) Simulated photorefraction luminance gradients magnified and minified by magnitudes equivalent to those induced by ±6D of trial lenses. Panel (**B**) The luminance gradient slope plotted as a function of the image magnification for the four different gradient profiles, clearly indicating the impact of optical magnification/minification on all the non-zero gradient profiles. Panel (**C**) The dioptric output expected out of the photorefractor for different values of image magnification/minification for ±6D of trial lenses. Panel (**D**) Mean (±1SD) difference in the refractive power measured by the photorefractor for different levels of induced magnification/minification, relative to no induced magnification in eyes wearing the afocal magnifier. Panel (**E**) The same data as panel (**D**) but for eyes without the afocal magnifier. The dashed horizontal line indicates no change in the refractive power estimate of the photorefractor with induced magnification/minification. The underestimation of myopia for magnification and overestimation of myopia for minification is evident in panel (**D**). Figure adapted with permission from Bharadwaj et al. [64] © Optica Publishing Group.

3.3. The Dead Zone in Photorefraction

Eccentric photorefraction relies on analyzing the crescent (for single light source) or the luminance slope (for multiple light sources) that appears in the pupil (Figures 1 and 2). In the former type of photorefractors, there exists a refractive error range within which the crescent is not observable. This range is termed the ‘dead zone’. The limits of the dead zone are defined by the relative defocus values that result in the beginning of the crescent just at the margin of the pupil, that is, $y_b = \pm R$. The $+$ and $-$ signs apply for $D_r < 0$ and $D_r > 0$ respectively. Consequently, this establishes a dead zone centered at $D_r = 0$ and a width of value $w = e/(RA)$. Using Equation (1), the dead zone limits for the relative defocus can be converted into a spherical refractive error:

$$S_1 = -\frac{1}{A} - \frac{e}{2RA} \qquad S_2 = -\frac{1}{A} + \frac{e}{2RA}$$

In terms of the spherical refractive error, the dead zone expands over a range of w diopters centered at $S = -1/A$. Considering that in typical photorefraction practice $A \approx 1$ m, this affects low myopes.

It is always desirable to have the smallest possible dead zone, which can be achieved by reducing the ratio e/A. As the e/A ratio decreases, the extent of the dead zone reduces. However, it is also noted that this reduction occurs at the expense of increasing the rate at which the extent of the crescent approaches an asymptote, thereby limiting the effective working range of the technique. Nevertheless, the extent of the dead zone is often smaller than predicted by this geometrical approach. One reason for this discrepancy is that the light source is never point-like. Consequently, this reduces the effective value of eccentricity, thus impacting the e/A ratio. For eccentric photorefractors that utilize multiple light sources simultaneously to measure the slope [5,7], the dead zone is significantly reduced or even nonexistent. Other reasons for a reduced dead zone might be the presence of optical aberrations or light scattered within the eye—these factors are discussed in detail by Bobier and Braddick [5].

In general, the dioptric range of the dead zone and the overall operating range of photorefraction depend on the eccentricity of the infrared light source from the camera aperture. Larger eccentricity of the light source results in wider dead zones but also wider operating ranges. Closer eccentricities of the light source result in the opposite effect. So, in theory, the operating range of the photorefractor can be extended to include higher refractive errors (e.g., > ±7D), but at the cost of this technique becoming insensitive to smaller refractive errors. While this may not be possible with commercial photorefractors that come with a fixed distance between the light source and the camera apertures, custom-designed photorefractors used for research purposes may build in this functionality depending on the cohort being examined.

The existence of the dead zone, which may be considered a limitation of the technique, can also be conveniently exploited. The center of the dead zone corresponds to a defocus in the eye, such that the retina and the camera are optically conjugated. Controlled amounts of defocus can then be added to the eye until this condition is met. From here, the spherical refractive error of the eye can be estimated. Following this approach, Roorda and colleagues devised an eccentric photo-optometer based on a moving camera behind a Badal optometer [67].

4. Outlook and Prospects

Through the past seven decades of evolution, photorefraction has become the technology of choice for the screening of uncorrected refractive errors and other amblyogenic factors in the pediatric population and for research endeavors assessing accommodation and the near-triadic behavior. Despite this, there is certainly room for improvement both in technology and in its usage scope. These improvements will meet the dual-purpose of improving the accuracy of the refraction estimates obtained using photorefraction and democratizing eye care by making this technique more cost effective, more accessible and enabling detection of a wider scope of ophthalmic dysfunctions. For instance, recent works have reported the implementation of photorefraction using smartphones [68–70]. In recent years, smartphones with built-in cameras and an eccentric light source relative to the camera have achieved performance comparable to those used in the optical laboratory. The computational capabilities of these smartphones have grown enormously, making them ideal candidates for several biomedical applications, including eccentric photorefraction. Certain challenges involving the utilization of the images captured by these smartphones for eccentric photorefraction need to be addressed—first, the photorefraction images may not only show the effect of the refractive error, but they are also often affected by uncontrolled amounts of intraocular scattering and/or optical aberrations that impact the accuracy of the method. Second, the resolution of the cropped image of the pupil is small and may be affected by noise because the images must be taken in a low-light environment. Advances in imaging techniques combined with computational techniques such as machine learning [69,70] or deep learning [71,72] may hold key solutions for these challenges.

Utilizing the photorefraction technique to identify corneal optical pathologies like keratoconus (Figure 6) [29,30] or near-vision dysfunctions like the spasm of near reflex [73,74] are examples of how the use of photorefraction may be extended beyond the screening of simple uncorrected refractive errors. Presently, the identification of the aforesaid conditions is reliant on technology that is very complex to implement, expensive, time-consuming and reliant of highly trained human resource [75]. All these preclude easy identification of these conditions in mass eye screening endeavors; perhaps, for the same reason, solid data on the prevalence and incidence of these conditions in the general public are not available from many parts of the world [75]. The advantages of photorefraction, listed in Section 1 of this review, allow overcoming several of the aforesaid challenges with the existing technology. Yet, other than the isolated reports noted above, the utility of photorefraction remains largely confined to one of screening uncorrected refractive errors. A concerted effort is needed from vision scientists, clinicians and industry partners to overcome this barrier and establish photorefraction as a screening tool for other ophthalmic diseases of public health relevance.

Author Contributions

S.R.B.: Conceptualization, Visualization, Writing—original draft preparation, Writing—reviewing and editing; S.M.: Conceptualization, Visualization, Writing—original draft preparation, Writing—reviewing and editing; P.A.: Conceptualization, Writing—reviewing and editing. All authors have read and agreed to the published version of the manuscript.

Funding

S.R.B. was supported by the United States-India Educational Foundation (USIEF) for a Fulbright-Nehru Academic and Professional Excellence Fellowship during the writing phase of the study.

Institutional Review Board Statement

Not applicable.

Informed Consent Statement

Not applicable.

Data Availability Statement

Not applicable.

Acknowledgments

S.R.B. would like to thank Hyderabad Eye Research Foundation, L V Prasad Eye Institute for financially supporting his research on photorefraction. S.R.B. would also like to thank the United States-India Educational Foundation (USIEF) for a Fulbright-Nehru Academic and Professional Excellence Fellowship during the writing phase of the study.

Conflicts of Interest

The authors declare no conflict of interest.

References

1. Howland, H.C. Photorefraction of eyes: History and future prospects. *Optom. Vis. Sci.* **2009**, *86*, 603–606. https://doi.org/10.1097/OPX.0b013e3181a523c9.
2. Howland, H.C.; Braddick, O.; Atkinson, J.; et al. Optics of photorefraction: Orthogonal and isotropic methods. *J. Opt. Soc. Am.* **1983**, *73*, 1701–1708. https://doi.org/10.1364/josa.73.001701.
3. Kaakinen, K. A simple method for screening of children with strabismus, anisometropia or ametropia by simultaneous photography of the corneal and the fundus reflexes. *Acta Ophthalmol.* **1979**, *57*, 161–171. https://doi.org/10.1111/j.1755-3768.1979.tb00481.x.
4. Kaakinen, K.; Tommila, V. A clinical study on the detection of strabismus, anisometropia or ametropia of children by simultaneous photography of the corneal and the fundus reflexes. *Acta Ophthalmol.* **1979**, *57*, 600–611. https://doi.org/10.1111/j.1755-3768.1979.tb00507.x.
5. Bobier, W.R.; Braddick, O.J. Eccentric photorefraction: Optical analysis and empirical measures. *Am. J. Optom. Physiol. Opt.* **1985**, *62*, 614–620.
6. Norcia, A.M.; Zadnik, K.; Day, S.H. Photorefraction with a catadioptric lens. Improvement on the method of Kaakinen. *Acta Ophthalmol.* **1986**, *64*, 379–385. https://doi.org/10.1111/j.1755-3768.1986.tb06939.x.
7. Schaeffel, F.; Wilhelm, H.; Zrenner, E. Inter-individual variability in the dynamics of natural accommodation in humans: Relation to age and refractive errors. *J. Physiol.* **1993**, *461*, 301–320.
8. Kaur, K.; Gurnani, B. *Slit-Lamp Biomicroscope*; StatPearls Publishing LLC: St. Petersburg, FL, USA, 2024.
9. Schaeffel, F.; Farkas, L.; Howland, H.C. Infrared photoretinoscope. *Appl. Opt.* **1987**, *26*, 1505–1509. https://doi.org/10.1364/AO.26.001505.
10. Bharadwaj, S.R.; Sravani, N.G.; Little, J.A.; et al. Empirical variability in the calibration of slope-based eccentric photorefraction. *J. Opt. Soc. Am. A Opt. Image Sci. Vis.* **2013**, *30*, 923–931. https://doi.org/10.1364/JOSAA.30.000923.

11. Campbell, M.C.; Bobier, W.R.; Roorda, A. Effect of monochromatic aberrations on photorefractive patterns. *J. Opt. Soc. Am. A Opt. Image Sci. Vis.* **1995**, *12*, 1637–1646. https://doi.org/10.1364/josaa.12.001637.
12. Roorda, A.; Campbell, M.C.; Bobier, W.R. Slope-based eccentric photorefraction: Theoretical analysis of different light source configurations and effects of ocular aberrations. *J. Opt. Soc. Am. A Opt. Image Sci. Vis.* **1997**, *14*, 2547–2556. https://doi.org/10.1364/josaa.14.002547.
13. Wu, Y.; Thibos, L.N.; Candy, T.R. Two-dimensional simulation of eccentric photorefraction images for ametropes: Factors influencing the measurement. *Ophthalmic Physiol. Opt.* **2018**, *38*, 432–446. https://doi.org/10.1111/opo.12563.
14. Ferreira, A.; Vieira, R.; Maia, S.; et al. Photoscreening for amblyopia risk factors assessment in young children: A systematic review with meta-analysis. *Eur. J. Ophthalmol.* **2023**, *33*, 92–103. https://doi.org/10.1177/11206721221099777.
15. Horwood, A.M.; Griffiths, H.J.; Carlton, J.; et al. Scope and costs of autorefraction and photoscreening for childhood amblyopia-a systematic narrative review in relation to the EUSCREEN project data. *Eye* **2021**, *35*, 739–752. https://doi.org/10.1038/s41433-020-01261-8.
16. Silverstein, E.; Donahue, S.P. Preschool Vision Screening: Where We Have Been and Where We Are Going. *Am. J. Ophthalmol.* **2018**, *194*, xviii–xxiii. https://doi.org/10.1016/j.ajo.2018.07.022.
17. Bharadwaj, S.R.; Wang, J.; Candy, T.R. Pupil responses to near visual demand during human visual development. *J. Vis.* **2011**, *11*, 6. https://doi.org/10.1167/11.4.6.
18. Horwood, A.M.; Riddell, P.M. Developmental changes in the balance of disparity, blur, and looming/proximity cues to drive ocular alignment and focus. *Perception* **2013**, *42*, 693–715. https://doi.org/10.1068/p7506.
19. Kasthurirangan, S.; Glasser, A. Age related changes in accommodative dynamics in humans. *Vision. Res.* **2006**, *46*, 1507–1519. https://doi.org/10.1016/j.visres.2005.11.012.
20. Toor, S.; Horwood, A.; Riddell, P. The effect of asymmetrical accommodation on anisometropic amblyopia treatment outcomes. *J. AAPOS* **2019**, *23*, 203.e1–203.e5. https://doi.org/10.1016/j.jaapos.2019.05.010.
21. Barathi, V.A.; Beuerman, R.W.; Schaeffel, F. Effects of unilateral topical atropine on binocular pupil responses and eye growth in mice. *Vision. Res.* **2009**, *49*, 383–387. https://doi.org/10.1016/j.visres.2008.11.005.
22. Bossong, H.; Swann, M.; Glasser, A.; et al. Applicability of infrared photorefraction for measurement of accommodation in awake-behaving normal and strabismic monkeys. *Investig. Ophthalmol. Vis. Sci.* **2009**, *50*, 966–973. https://doi.org/10.1167/iovs.08-2686.
23. Feldkaemper, M.P.; Schaeffel, F. Evidence for a potential role of glucagon during eye growth regulation in chicks. *Vis. Neurosci.* **2002**, *19*, 755–766. https://doi.org/10.1017/s0952523802196064.
24. Katzir, G.; Howland, H.C. Corneal power and underwater accommodation in great cormorants (Phalacrocorax carbo sinensis). *J. Exp. Biol.* **2003**, *206*, 833–841. https://doi.org/10.1242/jeb.00142.
25. Machovsky-Capuska, G.E.; Howland, H.C.; Raubenheimer, D.; et al. Visual accommodation and active pursuit of prey underwater in a plunge-diving bird: The Australasian gannet. *Proc. Biol. Sci.* **2012**, *279*, 4118–4125. https://doi.org/10.1098/rspb.2012.1519.
26. Troilo, D.; Howland, H.C.; Judge, S.J. Visual optics and retinal cone topography in the common marmoset (Callithrix jacchus). *Vision. Res.* **1993**, *33*, 1301–1310. https://doi.org/10.1016/0042-6989(93)90038-x.
27. Vilupuru, A.S.; Kasthurirangan, S.; Glasser, A. Dynamics of accommodative fatigue in rhesus monkeys and humans. *Vision. Res.* **2005**, *45*, 181–191. https://doi.org/10.1016/j.visres.2004.07.036.
28. Duret, A.; Humphries, R.; Ramanujam, S.; et al. The infrared reflex: A potential new method for congenital cataract screening. *Eye* **2019**, *33*, 1865–1870. https://doi.org/10.1038/s41433-019-0509-9.
29. Chen, Y.L.; Tan, B.; Baker, K.; et al. Simulation of keratoconus observation in photorefraction. *Opt. Express* **2006**, *14*, 11477–11485. https://doi.org/10.1364/oe.14.011477.
30. Patel, A.M.; Kumar, P.; Vaddavalli, P.K.; et al. The Value of Eccentric Infrared Photorefraction in Evaluating Keratoconus. *Optom. Vis. Sci.* **2022**, *99*, 763–773. https://doi.org/10.1097/OPX.0000000000001940.
31. Thibos, L.N.; Hong, X.; Bradley, A.; et al. Statistical variation of aberration structure and image quality in a normal population of healthy eyes. *J. Opt. Soc. Am. A Opt. Image Sci. Vis.* **2002**, *19*, 2329–2348.
32. Chen, Y.C.; Jiang, C.J.; Yang, T.H.; et al. Development of a human eye model incorporated with intraocular scattering for visual performance assessment. *J. Biomed. Opt.* **2012**, *17*, 075009. https://doi.org/10.1117/1.JBO.17.7.075009.
33. Howland, H.C. Optics of photoretinoscopy: Results from ray tracing. *Am. J. Optom. Physiol. Opt.* **1985**, *62*, 621–625.
34. Howland, H.C.; Sayles, N. Photokeratometric and photorefractive measurements of astigmatism in infants and young children. *Vision. Res.* **1985**, *25*, 73–81. https://doi.org/10.1016/0042-6989(85)90082-3.
35. Sravani, N.G.; Nilagiri, V.K.; Bharadwaj, S.R. Photorefraction estimates of refractive power varies with the ethnic origin of human eyes. *Sci. Rep.* **2015**, *5*, 7976. https://doi.org/10.1038/srep07976.
36. Bharadwaj, S.R.; Candy, T.R. Cues for the control of ocular accommodation and vergence during postnatal human development. *J. Vis.* **2008**, *8*, 14. https://doi.org/10.1167/8.16.14.

37. Ntodie, M.; Bharadwaj, S.R.; Balaji, S.; et al. Comparison of Three Gaze-position Calibration Techniques in First Purkinje Image-based Eye Trackers. *Optom. Vis. Sci.* **2019**, *96*, 587–598. https://doi.org/10.1097/OPX.0000000000001405.
38. Schaeffel, F. Kappa and Hirschberg ratio measured with an automated video gaze tracker. *Optom. Vis. Sci.* **2002**, *79*, 329–334. https://doi.org/10.1097/00006324-200205000-00013.
39. Choi, M.; Weiss, S.; Schaeffel, F.; et al. Laboratory, clinical, and kindergarten test of a new eccentric infrared photorefractor (PowerRefractor). *Optom. Vis. Sci.* **2000**, *77*, 537–548. https://doi.org/10.1097/00006324-200010000-00008.
40. Schaeffel, F.; Mathis, U.; Bruggemann, G. Noncycloplegic photorefractive screening in pre-school children with the "PowerRefractor" in a pediatric practice. *Optom. Vis. Sci.* **2007**, *84*, 630–639. https://doi.org/10.1097/OPX.0b013e3180dc99ea.
41. Gabriel, G.M.; Mutti, D.O. Evaluation of infant accommodation using retinoscopy and photoretinoscopy. *Optom. Vis. Sci.* **2009**, *86*, 208–215. https://doi.org/10.1097/OPX.0b013e3181960652.
42. Gehring, A.M.; Haensel, J.X.; Curtiss, M.K.; et al. Validation of the PowerRef 3 for Measuring Accommodation: Comparison With the Grand Seiko WAM-5500A Autorefractor. *Transl. Vis. Sci. Technol.* **2022**, *11*, 25. https://doi.org/10.1167/tvst.11.10.25.
43. Seidemann, A.; Schaeffel, F. An evaluation of the lag of accommodation using photorefraction. *Vision. Res.* **2003**, *43*, 419–430. https://doi.org/10.1016/s0042-6989(02)00571-0.
44. Bharadwaj, S.R.; Candy, T.R. Accommodative and vergence responses to conflicting blur and disparity stimuli during development. *J. Vis.* **2009**, *9*, 4. https://doi.org/10.1167/9.11.4.
45. Blade, P.J.; Candy, T.R. Validation of the PowerRefractor for measuring human infant refraction. *Optom. Vis. Sci.* **2006**, *83*, 346–353. https://doi.org/10.1097/01.opx.0000221402.35099.fb.
46. Ghahghaei, S.; Reed, O.; Candy, T.R.; et al. Calibration of the PlusOptix PowerRef 3 with change in viewing distance, adult age and refractive error. *Ophthalmic Physiol. Opt.* **2019**, *39*, 253–259. https://doi.org/10.1111/opo.12631.
47. Horwood, A.M.; Riddell, P.M. Can misalignments in typical infants be used as a model for infantile esotropia? *Investig. Ophthalmol. Vis. Sci.* **2004**, *45*, 714–720. https://doi.org/10.1167/iovs.03-0454.
48. Gekeler, F.; Schaeffel, F.; Howland, H.C.; et al. Measurement of astigmatism by automated infrared photoretinoscopy. *Optom. Vis. Sci.* **1997**, *74*, 472–482. https://doi.org/10.1097/00006324-199707000-00013.
49. Bharadwaj, S.R.; Schor, C.M. Acceleration characteristics of human ocular accommodation. *Vision. Res.* **2005**, *45*, 17–28. https://doi.org/10.1016/j.visres.2004.07.040.
50. Tondel, G.M.; Candy, T.R. Accommodation and vergence latencies in human infants. *Vision. Res.* **2008**, *48*, 564–576. https://doi.org/10.1016/j.visres.2007.11.016.
51. Marran, L.; Schor, C.M. Lens induced aniso-accommodation. *Vision. Res.* **1998**, *38*, 3601–3619. https://doi.org/10.1016/s0042-6989(98)00064-9.
52. Sravani, N.G.; Bharadwaj, S.R. Ocular Focusing Behavior of the One-Eyed Child. *Optom. Vis. Sci.* **2017**, *94*, 150–158. https://doi.org/10.1097/OPX.0000000000001009.
53. Pophal, C.J.; Trivedi, R.H.; Bowsher, J.D.; et al. Effectiveness of the Spot (tm) Vision Screener With Variations in Ocular Pigments. *Am. J. Ophthalmol.* **2024**, *264*, 99–103. https://doi.org/10.1016/j.ajo.2024.03.018.
54. Tabernero, J.; Ohlendorf, A.; Fischer, M.D.; et al. Peripheral refraction profiles in subjects with low foveal refractive errors. *Optom. Vis. Sci.* **2011**, *88*, E388–E394. https://doi.org/10.1097/OPX.0b013e31820bb0f5.
55. Tabernero, J.; Schaeffel, F. Fast scanning photoretinoscope for measuring peripheral refraction as a function of accommodation. *J. Opt. Soc. Am. A Opt. Image Sci. Vis.* **2009**, *26*, 2206–2210. https://doi.org/10.1364/JOSAA.26.002206.
56. Marshall, J.; Gole, G.A. Unilateral leukocoria in off axis flash photographs of normal eyes. *Am. J. Ophthalmol.* **2003**, *135*, 709–711. https://doi.org/10.1016/s0002-9394(02)02079-2.
57. Asensio-Sanchez, V.M.; Diaz-Cabanas, L.; Martin-Prieto, A. Photoleukocoria with smartphone photographs. *Int. Med. Case Rep. J.* **2018**, *11*, 117–119. https://doi.org/10.2147/IMCRJ.S163735.
58. Nilagiri, V.K.; Metlapally, S.; Schor, C.M.; et al. A computational analysis of retinal image quality in eyes with keratoconus. *Sci. Rep.* **2020**, *10*, 1321. https://doi.org/10.1038/s41598-020-57993-w.
59. Pantanelli, S.; MacRae, S.; Jeong, T.M.; et al. Characterizing the wave aberration in eyes with keratoconus or penetrating keratoplasty using a high-dynamic range wavefront sensor. *Ophthalmology* **2007**, *114*, 2013–2021. https://doi.org/10.1016/j.ophtha.2007.01.008.
60. Sarkar, S.; Devi, P.; Vaddavalli, P.K.; et al. Differences in Image Quality after Three Laser Keratorefractive Procedures for Myopia. *Optom. Vis. Sci.* **2022**, *99*, 137–149. https://doi.org/10.1097/OPX.0000000000001850.
61. Sarkar, S.; Vaddavalli, P.K.; Bharadwaj, S.R. Image Quality Analysis of Eyes Undergoing LASER Refractive Surgery. *PLoS ONE* **2016**, *11*, e0148085. https://doi.org/10.1371/journal.pone.0148085.
62. Devkar, K.; Arunkumar, S.; Bhakta, T.; et al. Explainable XceptionNet-Based Keratoconus Detection Using Infrared Images and Edge Computing. *IEEE Sens. Lett.* **2024**, *9*, 6000404, https://doi.org/10.1109/LSENS.2024.3509503.

63. Rabbetts, R.B. Subsidiary effects of correcting lenses; magnifying devices. In *Bennett & Rabbetts' Clinical Visual Optics*, 4th ed.; Rabbetts, R.B., Ed.; Butterworth Heinemann: Edinburgh, UK, 2007; pp. 245–274.
64. Bharadwaj, S.R.; Bandela, P.K.; Nilagiri, V.K. Lens magnification affects the estimates of refractive error obtained using eccentric infrared photorefraction. *J. Opt. Soc. Am. A Opt. Image Sci. Vis.* **2018**, *35*, 908–915. https://doi.org/10.1364/JOSAA.35.000908.
65. Anderson, H.A.; Manny, R.E.; Glasser, A.; et al. Static and dynamic measurements of accommodation in individuals with down syndrome. *Investig. Ophthalmol. Vis. Sci.* **2011**, *52*, 310–317.
66. Doyle, L.; Saunders, K.J.; Little, J.A. Trying to see, failing to focus: Near visual impairment in Down syndrome. *Sci. Rep.* **2016**, *6*, 20444.
67. Roorda, A.; Bobier, W.R.; Campbell, M.C. An infrared eccentric photo-optometer. *Vision. Res.* **1998**, *38*, 1913–1924. https://doi.org/10.1016/s0042-6989(97)00424-0.
68. Chun, J.; Kim, Y.; Shin, K.Y.; et al. Deep Learning-Based Prediction of Refractive Error Using Photorefraction Images Captured by a Smartphone: Model Development and Validation Study. *JMIR Med. Inform.* **2020**, *8*, e16225. https://doi.org/10.2196/16225.
69. Kwok, T.C.K.; Shum, N.C.M.; Ngai, G.; et al. Democratizing Optometric Care: A Vision-Based, Data-Driven Approach to Automatic Refractive Error Measurement for Vision Screening. In Proceedings of the IEEE International Symposium on Multimedia (ISM), Miami, FL, USA, 14–16 December 2015; pp. 7–12. https://doi.org/10.1109/ISM.2015.55.
70. Yang, Z.; Fu, E.Y.; Ngai, G.; et al. Screening for refractive error with low-quality smartphone images. In Proceedings of the Proceedings of the 18th International Conference on Advances in Mobile Computing & Multimedia, Chiang Mai Thailand, 30 November–2 December 2020. https://doi.org/10.1145/3428690.3429175.
71. Linde, G.; Chalakkal, R.; Zhou, L.; et al. Automatic Refractive Error Estimation Using Deep Learning-Based Analysis of Red Reflex Images. *Diagnostics* **2023**, *13*, 2810. https://doi.org/10.3390/diagnostics13172810.
72. Xu, D.; Ding, S.; Zheng, T.; et al. Deep learning for predicting refractive error from multiple photorefraction images. *Biomed. Eng. Online* **2022**, *21*, 55. https://doi.org/10.1186/s12938-022-01025-3.
73. Bharadwaj, S.R.; Ravisankar, C.; Roy, S.; et al. Fluctuations of Steady-State Accommodation Is a Marker for Screening Spasm of Near Reflex. *Transl. Vis. Sci. Technol.* **2021**, *10*, 9. https://doi.org/10.1167/tvst.10.11.9.
74. Bharadwaj, S.R.; Roy, S.; Satgunam, P. Spasm of Near Reflex: Objective Assessment of the Near-Triad. *Investig. Ophthalmol. Vis. Sci.* **2020**, *61*, 18. https://doi.org/10.1167/iovs.61.8.18.
75. Santodomingo-Rubido, J.; Carracedo, G.; Suzaki, A.; et al. Keratoconus: An updated review. *Cont. Lens Anterior Eye* **2022**, *45*, 101559. https://doi.org/10.1016/j.clae.2021.101559.